DECENTRALIZED $\mathcal{H}_\infty$-BASED CONTROL STRATEGY FOR DC GRIDS

M. A. Hernández-Mejías[1], E. Rodriguez-Diaz[2], A. Sala[1], R. Blasco-Gimenez[1], G. Chaqués-Herraiz[1], J. M. Guerrero[2]

1. Inst U. Automática Informática Industrial (AI2). Universitat Politècnica de València. Cno Vera s/n, E-46022 Valencia, Spain.
e-mail : maher3@upv.es , asala@isa.upv.es , r.blasco@ieee.org , guschahe@alumni.upv.es
2. Department of Energy Technology, Aalborg University, 9220 Aalborg East, Denmark.
e-mail : erd@et.aau.dk , joz@et.aau.dk

Abstract - This paper presents an $\mathcal{H}_\infty$ control design for a DC-grid, considering limited information of the rest of the grid. Proposed strategy is compared with previously reported plug-and-play and droop controllers. The paper shows both PSCAD/EMTDC simulation and experimental results in a scaled prototype.

Keyword - $\mathcal{H}_\infty$-based control, DC-grid, power generating units (PGUs), droop controller, plug-and-play control.

1 INTRODUCTION

In recent years, DC-grids have gained more and more attention due to the increasing penetration of renewable sources and energy storage. The concept of *grid* refers to a set of loads, *Power Generating Units* (PGUs) and possibly *Energy Storage Systems* (ESSs), operating as a single controllable system that provides power to its local area [1]. Other reason of the interest in this kind of systems is because DC-grids do not have issues associated with synchronization, reactive power flows, harmonic currents, and dc/ac conversion losses, which are inherent in AC-grids [2]. DC-grids has many applications in several field such as, electrical vehicles, marine systems, efficiency in smart houses, etc [3].

Droop control techniques are widely employed in order to coordinate multiple sources, that are connected in parallel to a common bus, without communication between the sources. These controllers are designed using an outer voltage loop with an inner current loop [4], [5], where a virtual impedances is used to create a droop curve that relates the terminal voltage and current of the PGUs. By doing so, the power converter units emulate the behaviour of an impedance, which ensures stability once the PGUs are connected to the dc grid. In [5] a comparison of different droop control realization for DC-grid system is carried out. However, there exists some drawbacks in droop controllers applied to DC-grids, since both perfect bus voltage regulation (zero steady-state error) and equal power sharing cannot be obtained. In practice, a trade-off between power-sharing and voltage deviation (due to line impedance) is achieved [6].

An alternative class of decentralized controller named *Plug-and-Play* control (PnP), has been proposed in [7], [8]. The main feature of this kind of strategy is the possibility of plug-in (addition) or plug-out (remove) a PGUs of the grids, without the necessity of changing all local controllers. In this case, the control for each unit is designed via solving a convex optimization problem (linear matrix inequalities LMIs), based on information of the corresponding unit and the features of the power lines connecting to neighboring PGUs. In particular [8], when a PGU is plugged in or out, at most its neighboring must to change/update their controller, whereas in [7] it is not necessary, without spoiling the closed-loop stability of the whole system.

Several non-droop based controller for voltage control of grid systems have also been developed, ie., robust controller ([9], for the AC case) which proposes a methods to regulate the voltage of a single PGU (master), robust two-degree-of-freedom approach [10], multivariable voltage control scheme based on loop-shaping approaches, conventional and resonant PI controller [11].

In this paper a local decentralized $\mathcal{H}_\infty$-based controller for each PGU of the grid is proposed. It is assumed that each local controllers regulate the voltage at point of common coupling (PCC) and every PGU supports a local load whose topology and parameter are considered unknown. Nevertheless, the load current is assumed to be measurable [7], [8]. Comparison with other control strategies will be made.

The structure of the paper is as follows: next section presents the dynamic models of a DC-grid with two parallel PGUs. The design procedure of decentralized $\mathcal{H}_\infty$-based controller is given in Section 3. Simulation results are illustrates in Section 4 and finally, a conclusion section close the paper.

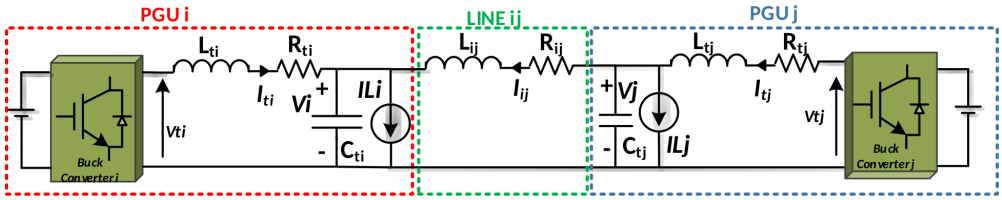

Fig. 1. Electrical scheme of two PGUs i, j and their interconnection via line ij.

2 Model of the DC-grid

Consider an islanded DC-grid, composed of N PGUs (power generating units). The interconnection between unit i and unit j is depicted in fig. 1. Each PGU is modelled as a DC voltage source (representing a generic renewable resources), a voltage-source converter (VSC), a RL filter and shunt capacitor ($R_{t_i}, L_{t_i}, C_{t_i}, i \in \{1, \ldots, N\}$), and finally, a local load IL_i whose topology and parameter are considered unknown [7],[8]. In fig. 1, $V_i, V_j, I_{t_i}, I_{t_j}, I_{L_i}, I_{L_j}, V_{t_i}, V_{t_j}$, are the load voltage at PCC_i and PCC_j, the filter currents, load currents, VSC terminal voltages, respectively and I_{ij} is the line current.

For the sake of simplicity, is this paper we will consider only a grid with 2 parallel PGUs. Applying Kirchoff's voltage law and Kirchoff's current law it is possible to get the following state equations:

$$PGU_1 : \begin{cases} \dfrac{dV_1}{dt} = \dfrac{1}{C_{t_1}}(I_{t1} - I_{12} - I_{L_1}) \\ \dfrac{dI_{t1}}{dt} = \dfrac{1}{L_{t1}}(-R_{t1}I_{t1} + V_{t1} - V_1) \end{cases} \quad (1)$$

$$PGU_2 : \begin{cases} \dfrac{dV_2}{dt} = \dfrac{1}{C_{t_2}}(I_{t2} + I_{12} - I_{L_2}) \\ \dfrac{dI_{t2}}{dt} = \dfrac{1}{L_{t2}}(-R_{t2}I_{t2} + V_{t2} - V_2) \end{cases} \quad (2)$$

$$Line_{12} : \begin{cases} \dfrac{dI_{12}}{dt} = \dfrac{1}{L_{12}}(V_1 - V_2 - R_{12}I_{12}) \end{cases} \quad (3)$$

Following the ideas presented in [7], [8], the load currents I_{L_i}, $i \in \{1, 2\}$ will be treated as a disturbance. For each PGU_i, $i \in \{1, 2\}$, we will represent its *local* dynamic as the following linear systems:

$$PGU_i : \begin{cases} \dot{x}_i(t) = A_i x_i(t) + B_i u(t) + M_i d(t) + H_i Q_i(t) \\ y(t) = C_i x(t) \end{cases} \quad (4)$$

where $x_i(t)$ is the 2-dimensional state vector associated to the PGU_i plus the line state (i.e., a third-order local dynamics), $d(t) = I_{L_i}$ is the load current disturbance (assumed to be measurable), and the voltage $V_j, j \neq i$ is considered a disturbance Q_i in order to carry out decentralized control. Note that this term corresponds to the coupling between both PGUs, as there is a disregarded interaction between the PGU's voltages.

For instance, the whole model equations for PGU_1 is given by equation (5) where an output equation (6) has been added indicating that V_1 and I_{t1} will be outputs of interest, actually measurable. A similar model would be available for PGU_2, omitted for brevity.

3 $\mathcal{H}_\infty$-based Control Procedure

The main objective of this section is to design a decentralized $\mathcal{H}_\infty$ controller for voltage and current loop in topology presented in fig. 1.

Fig. 2 shows the block diagram of the $\mathcal{H}_\infty$ control problem to be addressed in this work, where V_i^{ref}, n and y_m are the voltage reference, noise and output signals measured (with noise), respectively. The control structure of fig. 2 can be cast as a general control configuration (see fig. 3a), where $P(s)$ is called the *generalised* plant.

The main idea is to compute a stabilizing controller $K(s)$ to minimize the 2-norm of the output $\tilde{z} = [\tilde{z}_1, \tilde{z}_2]^T$ (see fig. 3b). It is well-know that, this it is equivalent to minimizing the $\mathcal{H}_\infty$-norm of the transfer function from w to $\tilde{z}$, [12]. The reader is referred to the cited work for ample detail on other $\mathcal{H}_\infty$ control applications to multivariable systems. Closed-loop transfer function from w to $\tilde{z}$ is given by the *linear fractional transformation* $\tilde{z} = F_l(Pw(s), K)w$, where:

$$F_l(Pw(s), K) := P_{w_{11}}(s) + P_{w_{12}}(s)K(I - P_{w_{22}}(s)K)^{-1}P_{w_{21}}(s) \quad (7)$$

with:

$$\begin{bmatrix} \tilde{z} \\ \cdots \\ v \end{bmatrix} = \begin{bmatrix} P_{w_{11}}(s) & P_{w_{12}}(s) \\ P_{w_{21}}(s) & P_{w_{22}}(s) \end{bmatrix} \begin{bmatrix} w \\ u \end{bmatrix} \quad (8)$$

The dimensions of the different elements of P_w are obtained from the size of the signals in fig. 2 and 3a. In particular, our generalised plant $P(s)$ is of dimensions 6×5 and that amounts to having the blocks in (8) of sizes: $[P_{w11}: 2 \times 4]$, $[P_{w12}: 4 \times 4]$, $[P_{w21}: 2 \times 1]$, $[P_{w22}: 4 \times 1]$. Note that in fig. 3b, all external inputs (references, disturbances, noise, etc) are denoted by w, $\tilde{z}$ denotes output signal to be minimized, u is the control vector that will be compute and $v = [y_m, V_i^{ref}]^T$ is the vector of measurements available to the controller.

Therefore, the $\mathcal{H}_\infty$-based control is formulated to minimize the closed-loop H_∞-norm, i.e.,:

$$\min_{K \ stabilizing} \left\| F_l(Pw(s), K) \right\|_\infty \quad (9)$$

$$\underbrace{\begin{bmatrix} \dot{V}_1 \\ \dot{I}_{t1} \\ \dot{I}_{12} \end{bmatrix}}_{\dot{x}(t)} = \underbrace{\begin{bmatrix} 0 & \frac{1}{C_{t1}} & -\frac{1}{C_{t1}} \\ -\frac{1}{L_{t1}} & -\frac{R_{t1}}{L_{t1}} & 0 \\ \frac{1}{L_{12}} & 0 & -\frac{R_{12}}{L_{12}} \end{bmatrix}}_{A_1} \underbrace{\begin{bmatrix} V_1 \\ I_{t1} \\ I_{12} \end{bmatrix}}_{x(t)} + \underbrace{\begin{bmatrix} 0 \\ \frac{1}{L_{t1}} \\ 0 \end{bmatrix}}_{B_1} \underbrace{V_{t1}}_{u(t)} + \underbrace{\begin{bmatrix} -\frac{1}{C_{t1}} \\ 0 \\ 0 \end{bmatrix}}_{M_1} \underbrace{I_{L_1}}_{d(t)} + \underbrace{\begin{bmatrix} 0 \\ 0 \\ -\frac{1}{L12} \end{bmatrix}}_{H_1} \underbrace{\begin{bmatrix} V_2 \end{bmatrix}}_{Q_1} \quad (5)$$

$$y(t) = \underbrace{\begin{bmatrix} 1 & 0 & 0 \\ 0 & 1 & 0 \end{bmatrix}}_{C_1} \begin{bmatrix} V_1 \\ I_{t1} \\ I_{12} \end{bmatrix} \quad (6)$$

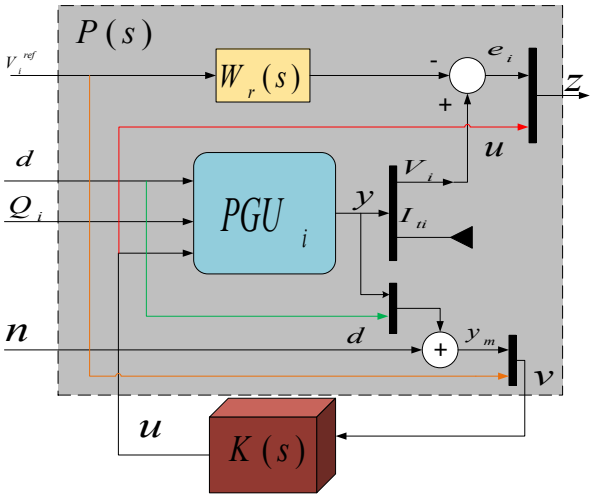

Fig. 2. The $\mathcal{H}_\infty$ control approach to be solved.

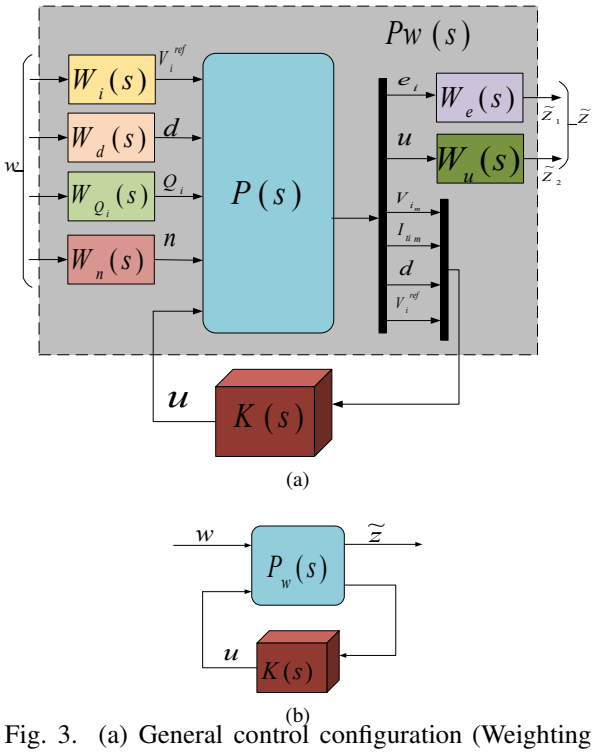

Fig. 3. (a) General control configuration (Weighting Generalised plant $Pw(s)$) and (b) The standard $\mathcal{H}_\infty$ configuration.

The problem can be suitably stated once the weighting functions have been selected properly for the application at hand, which is discussed next. To understand its importance, it is necessary to remember that the proposed H_∞-based controller tries to compute a controller $K(s)$ that keep the signal $\tilde{z}$ small, i.e., a frequency weight $W_e(s), W_u(s)$ that amplifies a signal in a certain band, would yield a controller that keeps the non-weighting signal e_i, u small in this band. Conversely, a frequency weight attenuating a signal in a band will keep a bigger the non-weighting signal in the closed-loop system.

3.1 Selection of weighting functions

A crucial requirement in the design of $\mathcal{H}_\infty$ controller is to select the weighting functions $W_e(s), W_u(s), W_i(s), W_d(s), W_{Q_i}(s), W_n(s)$ and $W_r(s)$.

Selection of $W_e(s)$: This weight modulates the desired tracking error compared to the reference model. It is usually a low-pass filter with high gain at low frequencies. In our case, we chose:

$$W_e(s) = \frac{s + 1200}{2s + 0.12} \quad (10)$$

whose Bode amplitude diagram appears in solid blue line in fig. 4.

Selection of $W_u(s)$: This weight is used to limit the control energy (amplitude) and bandwidth of the controller's output . Normally, a high-pass filter is chosen [12] in order to limit the high-frequency components of the controller but leaving more room for the low-frequency components for reduced steady-state error. In this particular case under study, we want to limit the control action increment to 12 V at low frequencies when disturbances and set-points have the frequency characteristics later detailed. However, in high frequencies, we want a smaller gain in order to attenuate the measurement noise n. An appropriate weighting function $W_u(s)$ for the system is given by transfer function (11) and is depicted in fig. 4 in dashed red line.

$$W_u(s) = \frac{1.259s + 0.7313}{s + 9.206} \quad (11)$$

Selection of $W_{ref}(s)$: This weight represents the reference/target model to which the closed-lopp system

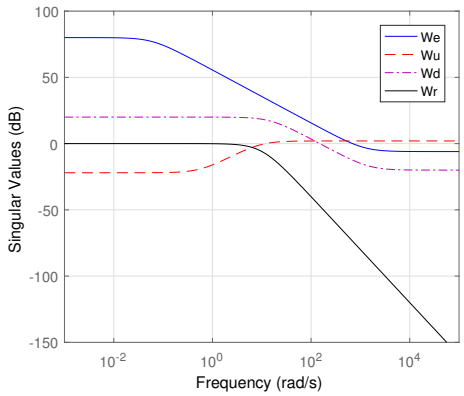

Fig. 4. Bode magnitude plot of weighting functions for construction of generalized plant in fig. 2.

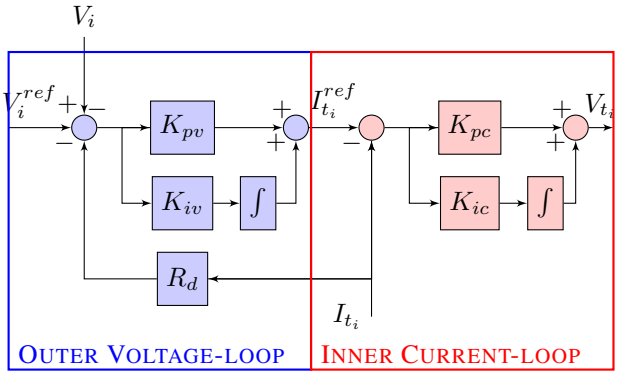

Fig. 5. Droop control diagram with outer-loop voltage and inner-loop current including virtual resistance R_d

I. Electrical parameters of $PGU_i,\ i \in \{1, 2\}$ and line parameters.

Parameter	Symbol	Value
DC power supply	V_{DC}	100 V
Shunt capacitance	C_{t_i}	1 mF
Series filter resistance	R_{t_i}	0.015 Ω
Series filter inductance	L_{t_i}	1.5 mH
Switching frequency	f_{sw}	5 KHz
Line inductance	L_{12}	0.22 mH
Line Resistance	R_{12}	10 Ω

should follows. In this case, we set the weight as a second order function with desired time constants and damping:

$$W_r(s) = \frac{1}{0.01s^2 + 0.198s + 1}, \tag{12}$$

The rest of weighting functions have been chosen as (see fig. 4):

$$W_n(s) = 0.1I_{3\times 3},\ W_i(s) = 1 \tag{13}$$

$$W_d(s) = \frac{0.1s + 150}{s + 15},\ W_Q(s) = 1 \tag{14}$$

4 Simulation Results

In order to verify the performance of the proposed control strategies let us consider the system depicted in fig. 1 with two PGUs. Simulations have been are carried out with PSCAD/EMTDC. The electrical and transmission lines parameters are listed in Table I. It is assumed that in each PGU there is a local load of 25 and 20 Ω, respectively (connected at a particular time in step load simulations). For a more realistic simulation results, we will consider noise in measurement voltage and current variables.

In order to show the effectiveness of the proposed $\mathcal{H}_\infty$-based controller, let us compare it with two different approaches. The first one corresponds to the well-known droop controller with virtual impedance depicted in fig. 5. In this case, the Buck converter is controlled by an inner mode current loop and outer voltage loop [5]. R_d corresponds to the virtual impedance which defines the droop relation between terminal voltages a currents PGUs: $K_{pv} = 0.5,\ K_{iv} = 100,\ K_{pc} = 1,\ K_{ic} = 10$ and $R_d = 0.1$.

The other control approach to be compare with the proposed one, is the plug-and-play controller presented in [8]. Solving problem 1 of this work is possible to compute the state-feedback matrix gains K_i for each local PnP controller shown in [8, fig. 1]. This matrix gain is given by:

$$K_i = [-1.2450\ -0.2658\ 21.0237],\ i \in \{1, 2\}$$

Now, it is possible to compute the $\mathcal{H}_\infty$ controller using the weighting functions $We(s), W_u(s), W_i(s), W_d(s), W_Q(s), W_n(s)$ and $W_{ref}(s)$ and solving the problem 9. The resulting controller achieves a $\mathcal{H}_\infty$-norm of 0.9496, for the closed-loop transfer function from w to z, which is less than one. In this case, a eighth-order controller is obtained.

4.1 Voltage reference tracking with step load response simulation

It is assumed that at the beginning ($t = 0\ s$), the PGUs are interconnected. The output voltage reference has been chosen equal for each unit, i.e., $V_1^{ref} = V_2^{ref} = 48\ V$. At time $t = 1.5\ s$ both local load are connected to the system. As can be seen from fig. 6 the proposed control has a good compensation of the current disturbance generated by the load, as well as, the good tracking of the reference signal at each PCC with very small steady-state errors. Note that, the dynamic response of the grid under droop controller has a steady-state error due to the value of the virtual resistance Rd, whereas the PnP controller achieves the desired tracking but with a slower dynamic. The control signals ap-

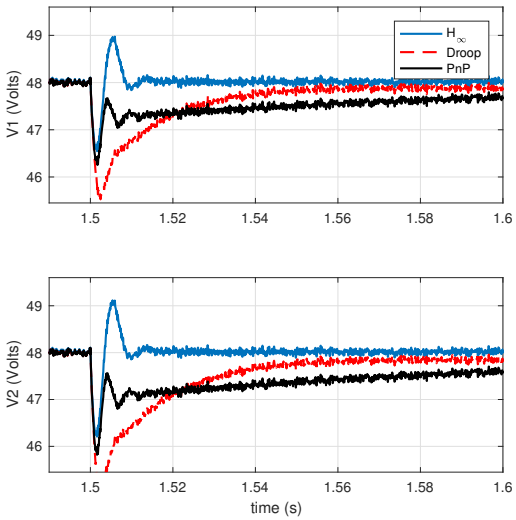

Fig. 6. Comparative of different control techniques. Step load at time 1.5 s. Top figure is Voltage at PCC_1, whereas button figure corresponds to voltage at PCC_2.

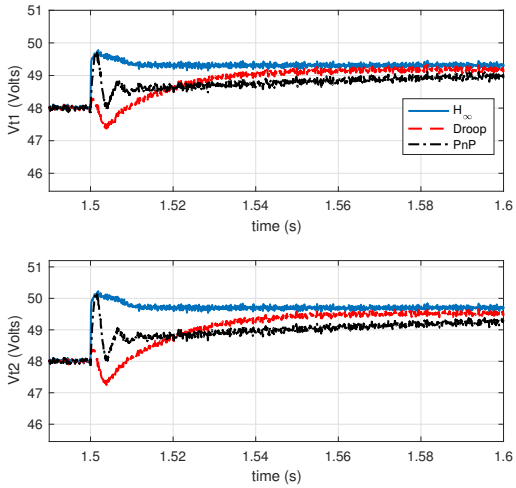

Fig. 7. Control action V_{t1} and V_{t2} applied to the units. Step load at time 1.5 s.

plied to the system are depicted in fig. 7. It can be noted that a higher control action is required by the proposed controller, however regarding a practical implementation this control action (duty cycle) still is feasible and well below the limits of the converter, therefore the improvement in the voltage regulation, shown in fig. 6, is worth a slight increment on the required control action.

5 Experimental Results

In this section, we utilize a experimental setup (see fig. 8), in order to illustrate and compare the dynamic closed-loop system with each control technique under study for tracking voltage reference with step-load test. In the experimental case, both PGUs are connected and supports a passive local load of 25 Ω for unit one and 20 Ω for unit two. Control application is programmed in Matlab/Simulink and compiled to a dSPACE controller

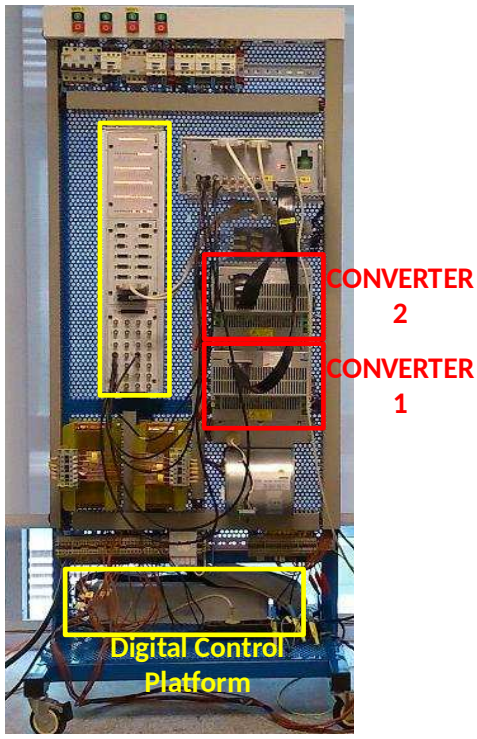

Fig. 8. Experimental platform.

board (R2013A). The experimental data are saved by ControlDesk software. The sampling period is 5 KHz as well as the PWM switching frequency. Fig. 9 shows, the voltage signal at each PCC for the proposed H_∞-control and droop configuration, during a step load test. As expected, the proposed H_∞-based control has a much better compensation of the disturbance than the other control and a small steady-state error. Fig. 10 shows the filter currents of both units.

6 Conclusion

A local decentralized $\mathcal{H}_\infty$-based control for DC-grid system has been proposed in this work. DC-grid consists of several PGUs connected in parallel at point of common coupling (PCC). Each PGU is modelled as a DC voltage source, a voltage source converter VSC, RL filter with shunt capacitor and finally a local load. A good response has been obtained with this controller, comparable to other widely-used techniques. The advantage of the $\mathcal{H}_\infty$ approach is that integration of structured and unstructured uncertainty for robustness analysis and μ-synthesis is easier than with other control structures; this will motivate future work in that direction.

Acknowledgements

This project has received funding from the *European Union's Horizon 2020 research and innovation program* under grant agreement No. 691714. The authors kindly acknowledge the financial support of Spanish Ministry of Economy and European Union FEDER

funds, under grants DPI2014-53245-R and DPI2016-81002-R (AEI/FEDER, UE).

REFERENCES

[1] T. AlSkaif, A. C. Luna, M. G. Zapata, J. M. Guerrero, and B. Bellalta, "Reputation-based joint scheduling of households appliances and storage in a microgrid with a shared battery," *Energy and Buildings*, vol. 138, pp. 228–239, 2017.

[2] E. Rodriguez-Diaz, F. Chen, J. C. Vasquez, J. M. Guerrero, R. Burgos, and D. Boroyevich, "Voltage-Level Selection of Future Two-Level LVdc Distribution Grids: A Compromise Between Grid Compatibiliy, Safety, and Efficiency," *IEEE Electrification Magazine*, vol. 4, no. 2, pp. 20–28, 2016.

[3] T. Dragicevic, X. Lu, J. C. Vasquez, and J. M. Guerrero, "Dc microgrids part ii: A review of power architectures, applications, and standardization issues," *IEEE transactions on power electronics*, vol. 5, no. 31, pp. 3528–3549, 2016.

[4] J. M. Guerrero, J. C. Vasquez, J. Matas, L. G. De Vicuña, and M. Castilla, "Hierarchical control of droop-controlled ac and dc microgrids. a general approach toward standardization," *IEEE Transactions on Industrial Electronics*, vol. 58, no. 1, pp. 158–172, 2011.

[5] F. Chen, R. Burgos, and D. Boroyevich, "Output impedance comparison of different droop control realizations in dc systems," in *2016 IEEE 17th Workshop on Control and Modeling for Power Electronics (COMPEL)*, pp. 1–6, June 2016.

[6] D. E. Olivares, A. Mehrizi-Sani, A. H. Etemadi, C. A. Cañizares, R. Iravani, M. Kazerani, A. H. Hajimiragha, O. Gomis-Bellmunt, M. Saeedifard, R. Palma-Behnke, *et al.*, "Trends in microgrid control," *IEEE Transactions on smart grid*, vol. 5, no. 4, pp. 1905–1919, 2014.

[7] M. S. Sadabadi, Q. Shafiee, and A. Karimi, "Plug-and-play voltage stabilization in inverter-interfaced microgrids via a robust control strategy," *IEEE Transactions on Control Systems Technology*, vol. PP, no. 99, pp. 1–11, 2016.

[8] M. Tucci, S. Riverso, and G. Ferrari-Trecate, "Voltage stabilization in dc microgrids through coupling-independent plug-and-play controllers," in *Decision and Control (CDC), 2016 IEEE 55th Conference on*, pp. 4944–4949, IEEE, 2016.

[9] R. Moradi, H. Karimi, and M. Karimi-Ghartemani, "Robust decentralized control for islanded operation of two radially connected dg systems," in *2010 IEEE International Symposium on Industrial Electronics*, pp. 2272–2277, IEEE, 2010.

[10] M. Babazadeh and H. Karimi, "A robust two-degree-of-freedom control strategy for an islanded microgrid," *IEEE transactions on power delivery*, vol. 28, no. 3, pp. 1339–1347, 2013.

[11] B. Bahrani, M. Saeedifard, A. Karimi, and A. Rufer, "A multivariable design methodology for voltage control of a single-dg-unit microgrid," *IEEE Transactions on Industrial Informatics*, vol. 9, no. 2, pp. 589–599, 2013.

[12] S. Skogestad and I. Postlethwaite, *Multivariable feedback control: analysis and design*, vol. 2. Wiley New York, 2007.

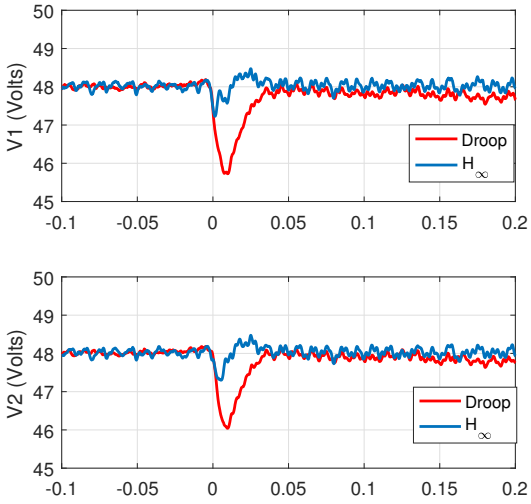

Fig. 9. Comparative of different control techniques. Step voltage reference change at time 1.5 s. Top figure is Voltage at PCC_1, whereas button figure corresponds to voltage at PCC_2.

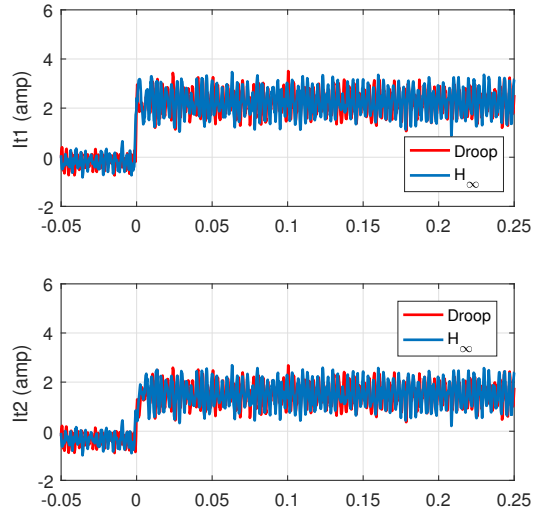

Fig. 10. Control actions V_{t1} and V_{t2} for step voltage reference at PCC_1.